An empirical model of the ionospheric sporadic E layer based on GNSS radio occultation data

AGU ADVANCING EARTH AND SPACE SCIENCE

Space Weather®

RESEARCH ARTICLE
10.1029/2022SW003113

An Empirical Model of the Ionospheric Sporadic E Layer Based on GNSS Radio Occultation Data

Bingkun Yu[1,2,3,4], Xianghui Xue[1,2,4,5,6,7], Christopher J. Scott[3], Xinan Yue[8], and Xiankang Dou[1,2,9]

[1]Deep Space Exploration Laboratory/School of Earth and Space Sciences, University of Science and Technology of China, Hefei, China, [2]CAS Key Laboratory of Geospace Environment, Department of Geophysics and Planetary Sciences, University of Science and Technology of China, Hefei, China, [3]Department of Meteorology, University of Reading, Berkshire, UK, [4]Anhui Mengcheng Geophysics National Observation and Research Station, University of Science and Technology of China, Hefei, China, [5]CAS Center for Excellence in Comparative Planetology, Hefei, China, [6]Hefei National Laboratory for the Physical Sciences at the Microscale, University of Science and Technology of China, Hefei, China, [7]Frontiers Science Center for Planetary Exploration and Emerging Technologies, University of Science and Technology of China, Hefei, China, [8]Key Laboratory of Earth and Planetary Physics, Institute of Geology and Geophysics, Chinese Academy of Sciences, Beijing, China, [9]Electronic Information School, Wuhan University, Wuhan, China

Key Points:

- An empirical model of the E_s layer is constructed, based on S4max data retrieved from Constellation Observing System for Meteorology, Ionosphere, and Climate satellite occultation measurements
- The model can provide the climatology of the intensity of E_s layers as a function of altitude, latitude, longitude, universal time, and day of year
- The correlation coefficients of hourly f_oEs and daily maximum f_oEs between observations and model are 0.52 and 0.68, respectively

Correspondence to:

B. Yu and X. Xue,
bkyu@ustc.edu.cn;
xuexh@ustc.edu.cn

Citation:

Yu, B., Xue, X., Scott, C. J., Yue, X., & Dou, X. (2022). An empirical model of the ionospheric sporadic E layer based on GNSS radio occultation data. *Space Weather*, *20*, e2022SW003113. https://doi.org/10.1029/2022SW003113

Received 5 APR 2022
Accepted 12 JUL 2022

Abstract

The intense plasma irregularities within the ionospheric sporadic E (E_s) layers at 90–130 km altitude have a significant impact on radio communications and navigation systems. As a result, the modeling of the E_s layer is very important for the accuracy, reliability, and further applications of modern real-time global navigation satellite system precise point positioning. In this study, we have constructed an empirical model of the E_s layer using the multivariable nonlinear least-squares-fitting method, based on the S4max from Constellation Observing System for Meteorology, Ionosphere, and Climate satellite radio occultation measurements in the period 2006–2014. The model can describe the climatology of the intensity of E_s layers as a function of altitude, latitude, longitude, universal time, and day of year. To validate the model, the outputs of the model were compared with ionosonde data. The correlation coefficients of the hourly f_oEs and the daily maximum f_oEs between the ground-based ionosonde observations and model outputs at Beijing are 0.52 and 0.68, respectively. The model can give a global climatology of the intensity of E_s layers and the seasonal variations of E_s layers, although the E_s layers during the summer are highly variable and difficult to accurately predict. The outputs of the model can be implemented in comprehensive models for a description of the climatology of E_s layers and provide relatively accurate information about the global variation of E_s layers.

Plain Language Summary

Sporadic E (E_s) layers are unusual clouds of intense ionization in the upper atmosphere. The E_s layer causes anomalous long-distance propagation of radio waves; thus, it can have a significant impact on wireless radio communications. The effects of the E_s layer on the global positioning system/global navigation satellite system (GNSS) radio occultation (RO) receivers can be used to study the global occurrence and intensity of E_s layers. Even though the formation mechanism of the midlatitude E_s layer is well-known and related to the ion vertical drift, its prediction is hard due to a large uncertainty in neutral winds from numerical models. In this study, we have constructed an empirical model of the E_s layer based on the maximum value of the amplitude scintillation S4 index (S4max) from GNSS RO observations during the period 2006–2014. A function is fitted to the S4max data to provide the empirical model outputs continuously in altitude, latitude, longitude, time of day, and day of year. The model performance is validated by ground-based ionosonde data. This model can be used for applications requiring global climatology of E_s layers or requiring the climatology of the E_s layer at some location far from the observing ionosondes.

1. Introduction

Ionospheric sporadic E (E_s) layers are abnormal thin-layered structures of high electron density in the E region between 90 and 130 km altitude. The E_s layer is remarkably thin, typically 0.1–10 km thick, and horizontally widespread, extending for more than 1,000 km (Qiu, Yu, et al., 2021; Tsai et al., 2018). The intense plasma irregularities within E_s layers can cause perturbations and scintillation in radio signals due to a large vertical gradient in electron density. The influences of E_s layers on radio communications are crucial for the accuracy, reliability, and further applications of modern real-time global navigation satellite system (GNSS) precise point positioning

(Yue et al., 2016). Because of the growing demand for reliable GNSS communication, position, navigation as well as the increasing use in GNSS applications in agriculture, avionics, sea, and location-based services (i.e., Fernandez-Prades et al., 2011), it is critical to track and predict these intense E-region plasma structures.

The most widely accepted mechanism for the formation of E_s layers at midlatitudes is vertical neutral wind shear (J. Mathews, 1998; Whitehead, 1961, 1970). The E_s layer is composed of long-lived metallic ions, such as Fe^+, Na^+, Mg^+, and Ca^+ (Kopp, 1997; Plane et al., 2015). Metallic ions converge vertically to form a thin layer of intense ionization, as a result of vertical shears in zonal and meridional neutral winds. Many theoretical and numerical modeling studies have shown that the spatial distributions of the occurrence and intensity of E_s layers are in general accordance with vertical ion convergence (VIC) by neutral wind shear (Arras et al., 2009; Chu et al., 2014; Koto et al., 1972; Niu, 2021a, 2021b; Qiu et al., 2019; Shinagawa et al., 2017; Yu et al., 2019). However, the wind shear theory does not account for the overall morphology of E_s layers (Tang, Zhou, et al., 2021; Whitehead, 1989), particularly the seasonal variability with a large summer maximum (Yu et al., 2019). The discrepancies between the VIC and E_s layers are attributed to the influences of other processes on the formation of E_s layers, for example, gravity wave breaking in the upper atmosphere (Guo & Liu, 2021; A. Z. Liu et al., 2013), global distribution and variation of metallic ions (Shinagawa et al., 2017), intense geomagnetic activities (Tang, Zhao, et al., 2021; Yu, Scott, Xue, Yue, Chi, et al., 2021), and chemical reactions of metallic ions (Plane, 2012; J. Wu et al., 2021). Additionally, without an available routine measurement of global high-resolution thermospheric winds, the wind shear process in the E region is typically provided using numerical models, making validation of the predicted winds practically difficult. Shinagawa et al. (2021) compared the VIC by wind shear obtained from the GAIA model with the observed critical frequencies of E_s layers (f_oEs) from an ionosonde. The correlation coefficient between daily average VIC and daily average f_oEs at 120 km altitude is 0.764, while the correlation coefficients at 110 and 130 km altitude are only 0.357 and 0.347, respectively. Thus, accurate forecasting is difficult to achieve. At present, the accuracy of the hourly f_oEs prediction by the numerical model is not sufficient. The correlation coefficient between the hourly f_oEs from ionosonde observations and hourly f_oEs from the model is 0.213 (Shinagawa et al., 2021).

The behavior of E_s layers is dominantly controlled by wind shear convergence nodes and the E_s layer presents pronounced 24-hr and 12-hr periodicities (Haldoupis, 2011; J. D. Mathews et al., 1997). J. Mathews (1998) proposed that the E_s layer is sporadic owing to instrumental limitations rather than physical properties. A sequential sporadic E layer has often been identified to appear by the Arecibo incoherent scatter radar. Based on GNSS radio occultation (RO) measurements from satellites, it has been confirmed that weak E_s layers are not spatially sporadic, and thus, the "sporadic" E layers should be more frequent than we thought (Yu et al., 2020; Yu, Scott, Xue, Yue, & Dou, 2021). A case of global simultaneous E_s layers was observed in a broad region by satellites and seven ground-based ionosondes (Yue et al., 2015). As a result, given that the E_s layer occurs frequently and periodically, it is reasonable to construct a model of the global climatology of E_s layers.

The ionospheric effects of plasma irregularities on GNSS signals from low Earth orbit-based receivers can be used to extract information on variations in electron density irregularities (Hu et al., 2014; Yue et al., 2016). The global occurrence and intensity of E_s layers have been widely investigated using GNSS RO signals (D. L. Wu et al., 2005; Arras et al., 2008; Chu et al., 2014; Z. Liu, Fang, et al., 2021; Tsai et al., 2018; Yu et al., 2019). Prediction of E_s layers remains rare, although it is practically important and widely studied. Recently, Yu, Xue, et al. (2021) proposed a generalized three-dimensional wind shear theory and found that a large-scale winter-to-summer interhemispheric transport of long-lived metallic ions is responsible for the seasonal dependence of E_s layers. Seasonal meridional transport plays an important role in the latitudinal distribution of E_s layers in different seasons and thus influences the climatology of E_s layers.

In this study, we have constructed an empirical model of the ionospheric E_s layer using the multivariable nonlinear least-squares-fitting method, based on GNSS RO measurements during 2006–2014 from the Constellation Observing System for Meteorology, Ionosphere, and Climate (COSMIC) satellites (Anthes et al., 2008). The model describes the climatology of E_s layers and represents the degree to which the E_s layer is sporadic and climatological. The model describes the E_s layer as a function of altitude, latitude, longitude, universal time (UT), and day of year (DOY). It can be implemented in comprehensive models for a description of the climatology of E_s layers and provide relatively accurate information about the global variation of E_s layers.

2. Radio Occultation Data

Ionospheric scintillation of radio signals occurs when a radio wave passes through plasma density irregularities in the ionosphere (Weber et al., 1985; Yue et al., 2014). The phase and amplitude scintillation in transionospheric radio signals are related to the temporal and spatial evolution of plasma irregularities. In general, the amplitude scintillation S4 index quantifies the amplitude of scintillation. The S4 index is defined as the standard deviation of the detrended intensity of received signals normalized to the average signal intensity (Briggs & Parkin, 1963), which is as follows:

$$S_4 = \frac{\sqrt{\left\langle \left(I - \overline{\langle I \rangle} \right)^2 \right\rangle}}{\overline{\langle I \rangle}}, \tag{1}$$

where I represents the square of the signal-to-noise ratio (SNR); and the bracket $\langle\ \rangle$ denotes the time average taken over one second. A low-pass temporal filter has been applied in $\langle I \rangle$ to obtain a new average of the intensity $\overline{\langle I \rangle}$ at each second.

The COSMIC mission is a constellation of six low Earth orbit satellites launched in April 2006 (Schreiner et al., 2007). The primary payload of each satellite is a global positioning system (GPS) RO receiver. Six COSMIC satellites were initially spaced sequentially in the same orbit at approximately 512 km before being raised to orbits at 800 km in the following 17 months. The COSMIC mission can provide 2000–2500 RO profiles every day, almost distributed evenly in local solar time (Yue et al., 2014). Long-term COSMIC S4 data have been processed and archived from the SNR intensity fluctuations of RO signals by the COSMIC Data Analysis and Archive Center (CDAAC) (Schreiner et al., 2011).

In the present study, the maximum values of amplitude scintillation S4 index (S4max) data occurring at 90–130 km altitudes over 9 years from 2006 to 2014 were used. The observations of S4max from COSMIC RO measurements have been used to investigate the climatology of the intensity of E_s layers (Qiu, Yu, et al., 2021; Yu et al., 2019). The S4max index correlates well with f_oEs measured from global ground-based ionosondes (Yu et al., 2020). The S4max occurring at E_s altitudes of 90–130 km is used as a proxy for the electron concentration within E_s layers (Arras & Wickert, 2018; L. C. A. Resende et al., 2018; Yu et al., 2020; Yu, Scott, Xue, Yue, & Dou, 2021).

3. Model Variables

We constructed an empirical model of the ionospheric E_s layer by a five-dimensional polynomial. The five variables are altitude (alt), geographic longitude (lon), geographic latitude (lat), UT, and DOY. These variables are used to represent the temporal and spatial variations in S4max on a global scale.

Figure 1 shows the density plot of S4max from COSMIC RO data with altitude in the period 2006–2014. The distribution of the probability of S4max is close to a typical Gaussian function of altitude with a peak at approximately 95 km. The distribution of S4max shows a gamma distribution. The number of S4max < 0.4 accounts for 73% of the S4max measurements ranging from 0 to 1. The blue crosses and yellow dots represent the mean and median S4max values at varying altitudes. The green line represents the curve over the mean S4max points fitted by a Gaussian function of altitude $y = 0.15 \cdot \exp\left(\frac{-(x-107.42)^2}{2\cdot 7.79^2}\right) + 0.22$. The variation in S4max shows that the intensity of the E_s layer has a Gaussian function of altitude with a peak approximately 107 km.

The winds play a fundamental role in the formation and dynamic process of E_s layers (Cai et al., 2017; Haldoupis, 2011; J. D. Mathews et al., 1997; Yuan et al., 2014). These thin electron density irregularities in the E region ionosphere have diurnal and semidiurnal periodicities (Cai et al., 2019; Pancheva et al., 2003). To study the local time variation in E_s layers, the left panel of Figure 2 shows the local time-longitude distribution of S4max from COSMIC RO measurements in the period 2006–2014. The green horizontal line represents 18 LT. The S4max daily maximum is at around 18 LT and the S4max daily minimum is at around 6 LT. The right panel of Figure 2 shows the UT-longitude distribution of S4max with the daily maximum occurring at 18 LT represented by the green lines. The occurrence and intensity of E_s layers exhibit strong diurnal and semidiurnal

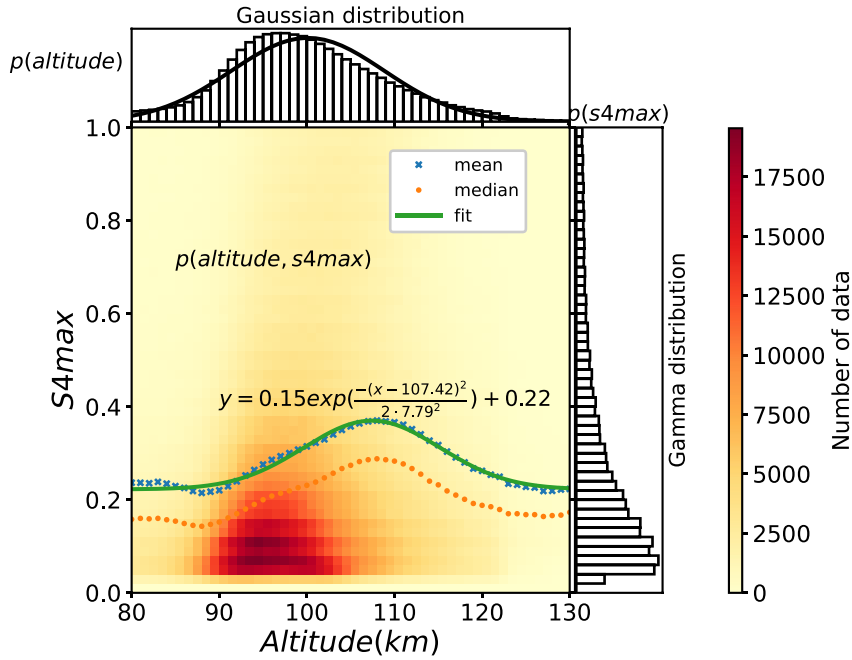

Figure 1. Density plot of S4max from Constellation Observing System for Meteorology, Ionosphere, and Climate radio occultationmeasurements with altitude in the period 2006–2014. The blue crosses and yellow dots represent the mean and median S4max values. The green line represents the curve over the mean S4max points fitted by a Gaussian function of altitude.

variations from RO measurements GNSS-RO satellite measurements (Y. Liu et al., 2018; D. L. Wu et al., 2005) and ground-based ionosondes (Pancheva et al., 2003; Pignalberi et al., 2014, 2015; Qiu, Zuo, et al., 2021; Šauli & Bourdillon, 2008; Whitehead, 1989). The low-latitude E_s layer presents a relatively strong diurnal variation and the midlatitude E_s layer presents a relatively strong semidiurnal variation (Chu et al., 2014; D. L. Wu et al., 2005; Yu et al., 2020).

Figure 3 shows the geographic latitude-DOY distribution of S4max and the geomagnetic latitude-DOY distribution of S4max from COSMIC RO measurements in the period 2006–2014. The seasonal dependence of E_s layers was found to be associated with the winter-to-summer interhemispheric transport of metallic ions by

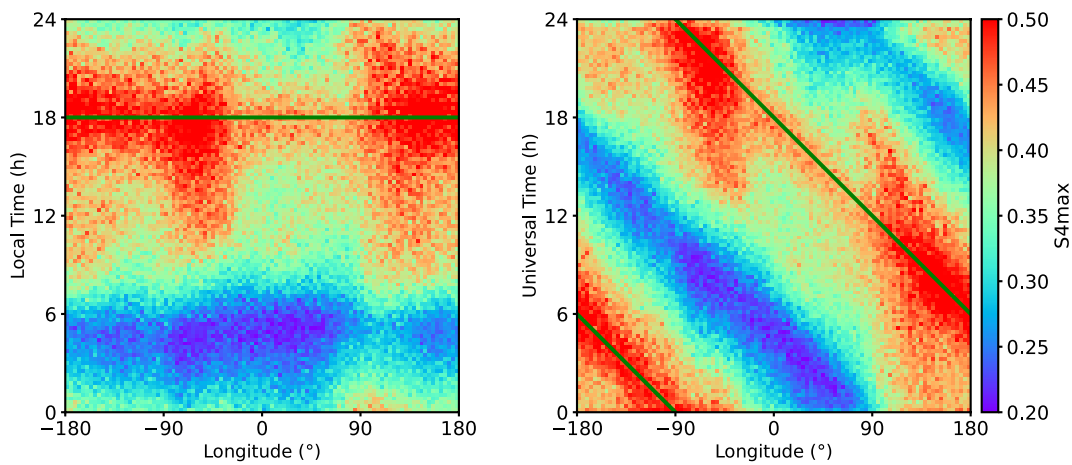

Figure 2. Left panel: local time-longitude distribution of S4max from Constellation Observing System for Meteorology, Ionosphere, and Climate radio occultation measurements in the period 2006–2014. The green horizontal line represents the diurnal variation in S4max with a daily maximum occurring at approximately 18 LT, which is also plotted in the right panel: universal time-longitude distribution of S4max.

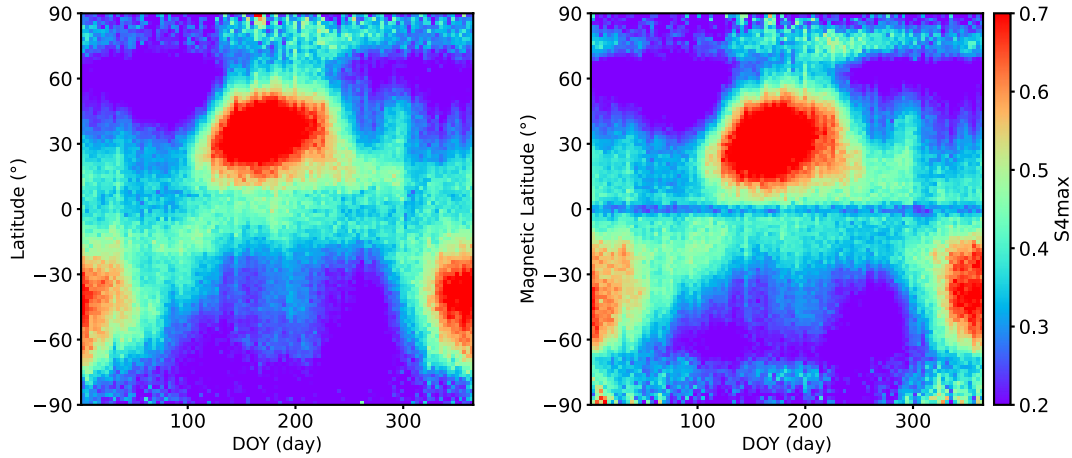

Figure 3. Left panel: geographic latitude-day of year (DOY) distribution of S4max from Constellation Observing System for Meteorology, Ionosphere, and Climate radio occultation measurements in the period 2006–2014. Right panel: geomagnetic latitude-DOY distribution of S4max.

the lower thermospheric meridional circulation (Yu, Xue, et al., 2021). In Figure 3, the E_s layer represented by S4max migrates from the southern midlatitudes of 30°S–60°S in January to the northern midlatitudes of 20°N–50°N in July, followed by transport backwards to the southern midlatitudes of 30°S–60°S in December. The E_s layer mainly resides over midlatitudes and is weaker at low-latitudes, particularly the gap near the equator (Yu et al., 2019). Therefore, we described the E_s layer as a function of latitude by a double-Gaussian fitting to exhibit the migration of E_s layers with DOY from the Southern Hemisphere to the Northern Hemisphere and the relatively strong E_s layers at midlatitudes.

Figure 4 shows the altitude-local time, altitude-DOY, altitude-latitude, and altitude-longitude distributions of S4max from COSMIC RO measurements in the period 2006–2014. S4max is a function of altitude by a Gaussian distribution as shown in Figure 1. In the second panel of Figure 4, the annual and semiannual periodic variations are found in the seasonal-to-interannual time series of S4max. The annual and semiannual variations in S4max were described using a 2-order trigonometric function of DOY.

Furthermore, the longitudinal wavenumber-4 (WN4) structure is observed in the occurrence and intensity of E_s layers at low latitudes and midlatitudes (Z. Liu, Fang, et al., 2021; Z. Liu, Li, et al., 2021; Niu, 2021b; Niu et al., 2019). The occurrence of the WN4 structures strongly depends on the season. Figure 5 shows the global distribution of S4max from COSMIC RO measurements in the spring (March, April, and May) and autumn (September, October, and November). A low S4max is observed near the geomagnetic equator. As a result of the parallel magnetic field preventing the ionized particles from efficiently vertically converging, the E_s layer is weak at the geomagnetic equator. The WN4 pattern of the E_s layer is very significant at low latitudes of 30°S–30°N. Therefore, the longitudinal variation in S4max was described using a 4-order trigonometric function of longitude.

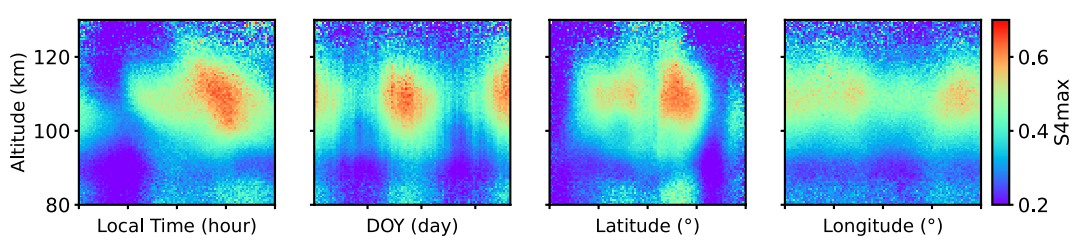

Figure 4. Left to right panels: altitude-local time, altitude-day of year, altitude-latitude, and altitude-longitude distributions of S4max from Constellation Observing System for Meteorology, Ionosphere, and Climate radio occultation measurements in the period 2006–2014.

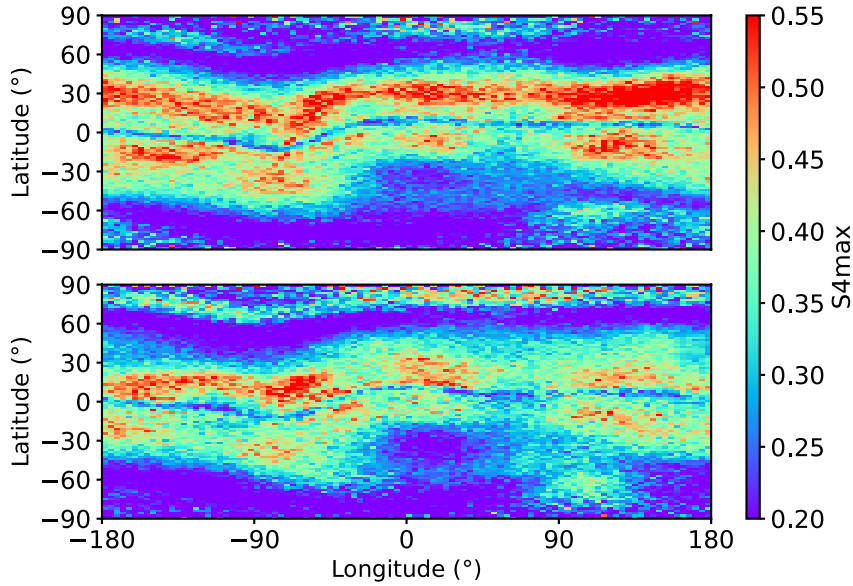

Figure 5. Global distribution of S4max from Constellation Observing System for Meteorology, Ionosphere, and Climate radio occultation measurements in the period 2006–2014. Plots for the spring (March, April, and May) in the top panel and the autumn (September, October, and November) in the bottom panel.

4. Mathematical Formulation

The empirical model of the E_s layer was constructed by a nonlinear least square fitting method based on S4max from COSMIC RO measurements in the period 2006–2014. The coefficient matrix of the nonlinear polynomial function is a least-square-approximation solution for all the S4max data points. This method has been applied to ionospheric empirical models, for example, the ionospheric electron density model (Kakinami et al., 2008), the total electron content (TEC) model (Jakowski et al., 2011), and the F2-layer peak density model (Z. Liu et al., 2019). The function of S4max was constructed using five variables as expressed below:

$$S4max = f_1(alt)f_2(UT)f_3(lat, DOY)f_4(lon)f_5(DOY), \tag{2}$$

The base functions from f_1 to f_5 are given as:

$$f_1 = a_0 + a_1 \exp\left(\frac{-(alt - a_2)^2}{2 \cdot a_3^2}\right), \tag{3}$$

$$f_2 = b_0 + \sum_{i=1}^{2} b_{1i} \cdot \cos\left(\frac{i2\pi \cdot (UT + lon/15 + b_{2i})}{24}\right), \tag{4}$$

$$f_3 = c_0 + c_1 \exp\left(\frac{-\left(lat - \left(c_2 \cdot \cos\left(\frac{2\pi \cdot (DOY + c_3)}{365.25}\right) + c_4\right)\right)^2}{2 \cdot c_5^2}\right) + c_6 \exp\left(\frac{-lat^2}{2 \cdot c_7}\right), \tag{5}$$

$$f_4 = d_0 + \sum_{i=1}^{4} d_{1i} \cdot \cos\left(\frac{i2\pi \cdot (lon + d_{2i})}{360}\right), \tag{6}$$

$$f_5 = e_0 + \sum_{i=1}^{2} e_{1i} \cdot \cos\left(\frac{i2\pi \cdot (DOY + e_{2i})}{365.25}\right), \tag{7}$$

The altitude variation of S4max was described by a Gaussian function of f_1. A 2-order trigonometric function was adopted in f_2 to describe the diurnal and semidiurnal variations. f_3 can capture the winter-to-summer inter-hemispheric movement of metallic ions, which contributes to the seasonal variation in E_s layers and considerable

Table 1
Summary of Base Functions and Parameters in the Model

Variable	Range	No. of CO-EFF	Function
Altitude	[90, 130]	4	$f_1 = 1.341 + 0.832exp\left(\frac{-(alt-108.219)^2}{2\cdot 8.195^2}\right)$
Universal Time	[0, 24]	5	$f_2 = 0.462 + 0.120\cdot\cos\left(\frac{2\pi\cdot(UT+lon/15+7.567)}{24}\right) + 0.029\cdot\cos\left(\frac{2\pi\cdot(UT+lon/15+2.610)}{12}\right)$
Latitude	[−90, 90]	8	$f_3 = 0.796 + 1.582exp\left(\frac{-\left(lat+32.774\cdot\cos\left(\frac{2\pi\cdot(DOY-0.206)}{365.25}\right)+0.723\right)^2}{2\cdot 32.368^2}\right) - 0.341exp\left(\frac{-lat^2}{2\cdot 12.099}\right)$
Longitude	[−180, 180]	9	$f_4 = 0.072 - 0.005\cdot\cos\left(\frac{2\pi\cdot(lon-6.705)}{360}\right) - 0.004\cdot\cos\left(\frac{2\pi\cdot(lon+144.419)}{180}\right)$ $- 0.0005\cdot\cos\left(\frac{2\pi\cdot(lon-4.033)}{120}\right) - 0.001\cdot\cos\left(\frac{2\pi\cdot(lon+11.302)}{90}\right)$
DOY	[1, 365]	5	$f_5 = 3.996 - 0.245\cdot\cos\left(\frac{2\pi\cdot(DOY+24.060)}{365.25}\right) + 0.900\cdot\cos\left(\frac{2\pi\cdot(DOY-178.470)}{182.625}\right)$

latitude dependence of the E_s layer that occurs predominantly at midlatitudes. The longitudinal variation is described by f_4. The annual and semiannual variations are described by f_5. The base functions from f_1 to f_5 and the corresponding parameters are shown in Table 1.

5. Model Results

Figure 6 shows the density scatter plot of S4max model outputs versus S4max observations. The correlation coefficient between S4max outputs and observations from RO measurements is 0.48. The model outputs are moderately correlated with the observations. The p value ($\ll$0.01) represents that the correlation coefficient has statistical significance. When the p value is smaller than 0.05, the correlation coefficient is considered to have statistical significance. The model overestimated small S4max values and underestimated large S4max values. This is because, in this study, the model provides a climatology of E_s layers, while other electrodynamic processes, for example, the neutral wind shear effect on the vertical motion of ions (Yu et al., 2019) and the geomagnetic activity effect on the significant periodic oscillations in E_s layers (Yu, Scott, Xue, Yue, Chi, et al., 2021), have not yet been included. Carmona et al. (2022) compared observations of E_s layers from five different GPS-RO techniques with ionosonde measurements over 8 years and found that the Yu et al. (2020) method, which uses the S4max index, shows better agreement with the measurements obtained from worldwide ground-based ionosondes. The results presented here show that the empirical model of E_s layers can be made using S4max from

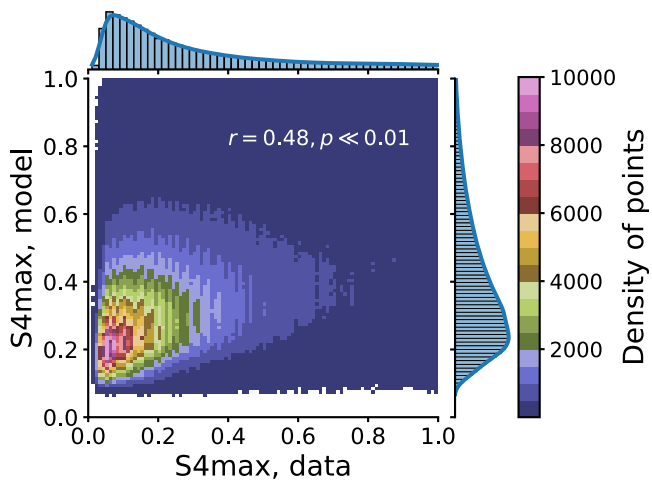

Figure 6. Density scatter plot of S4max model outputs versus S4max observations.

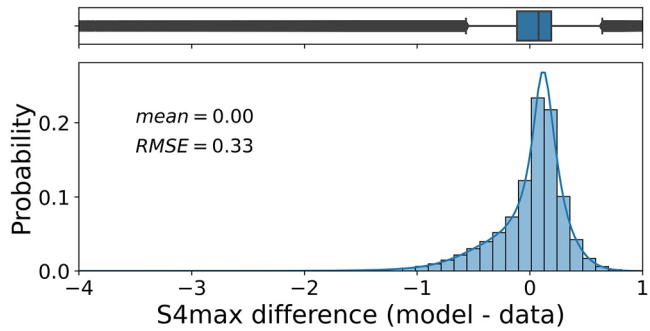

Figure 7. Statistical analyses of the difference between S4max model outputs and S4max observations in the period 2006–2014.

satellite RO measurements, although the prediction of E_s layers is severely constrained at present due to a lack of sufficient thermospheric wind data.

Figure 7 shows the statistical analyses of the difference between the S4max model outputs and S4max observations in the period 2006–2014. The S4max difference between the model and data shows a typical Gaussian distribution. The mean and the root mean square error are 0.00 and 0.33, respectively. The lower quartile is −0.113, while the upper quartile is 0.189, as seen in the box plot. Some points that fall outside of 1.5 times the inner quartile range, represented by black lines on both sides of the quartile box, indicate that some S4max values from the model outputs are overestimated and underestimated. The majority of outliers are found on the left side of the inner quartile range. The S4max from the model is often underestimated due to a lack of wind shear effects on the formation of intense E_s layers in the model.

To evaluate the model performance, the distributions of S4max from the model outputs are shown in Figures 8 and 9. Figures 8a and 8b show the local time-longitude and UT-longitude distributions of S4max from the model outputs, which are consistent with the S4max observations in Figure 2. In addition to the diurnal variation in the E_s layer, Figures 8c and 8d show the geographic latitude-DOY and geomagnetic latitude-DOY distributions from

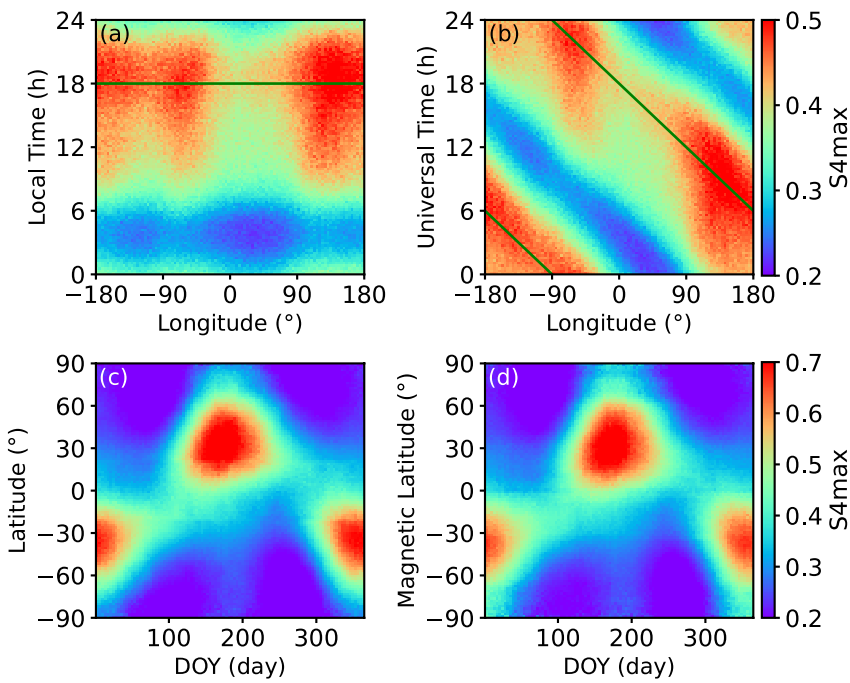

Figure 8. Results from model outputs: (a) local time-longitude, (b) universal time-longitude, (c) geographic latitude-day of year (DOY), and (d) geomagnetic latitude-DOY distributions of S4max.

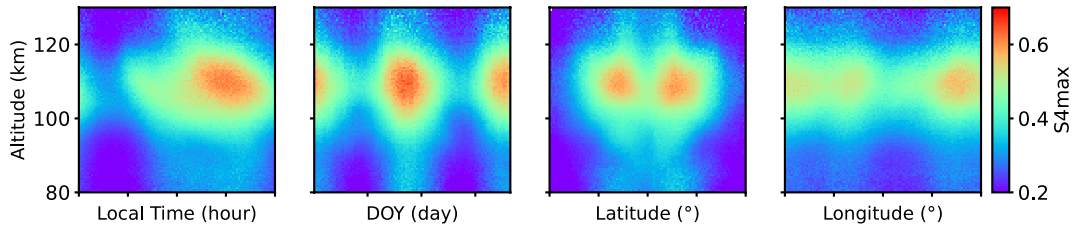

Figure 9. The same as Figure 4 but S4max from the model outputs.

the model. The latitudinal distributions of S4max show a meridional movement of E_s layers in the latitudes of ±60°, consistent with the distributions in Figure 3. The altitudinal distribution of S4max is a function of local time, DOY, latitude, and longitude. In comparison with S4max observations from RO measurements, the S4max altitudinal distributions from the model in Figure 9 generally agree with the observations in Figure 4. In addition, the model can describe the annual and semiannual variations of E_s layers.

Figure 10 shows the global distributions of the intensity of E_s layers at 0 UT in the four seasons, represented by S4max from satellite RO observations and the model outputs in the period 2006–2014. The morphologies of the E_s layers in the four seasons from the model agree with the observations. The seasonal variations dominate the variability of the E_s layers, with a maximum in the summer hemisphere and a minimum in the winter hemisphere. The intense E_s layer with S4max values exceeding 0.5 is predominantly distributed at midlatitudes. The E_s layer is weaker in the lower latitudes in both hemispheres. The weakest E_s layers with S4max values less than 0.1 can be found at 60°E longitude. These features of the climatology of E_s layers are reproduced by the model.

Figure 11 shows the global distributions of the intensity of E_s layers at 12 UT in the four seasons, represented by S4max from satellite RO observations and the model outputs in the period 2006–2014. The peaks of S4max values exceed 0.5 at 20°W and 120°E longitudes. The S4max minimum is at 120°W longitude. In addition to the seasonal variation in E_s layers, the model can also reproduce the longitudinal structure in the E_s layer, for example, the WN4 patterns as a result of the influence of lower atmospheric non-migrating tides (Z. Liu, Li, et al., 2021; Niu, 2021b).

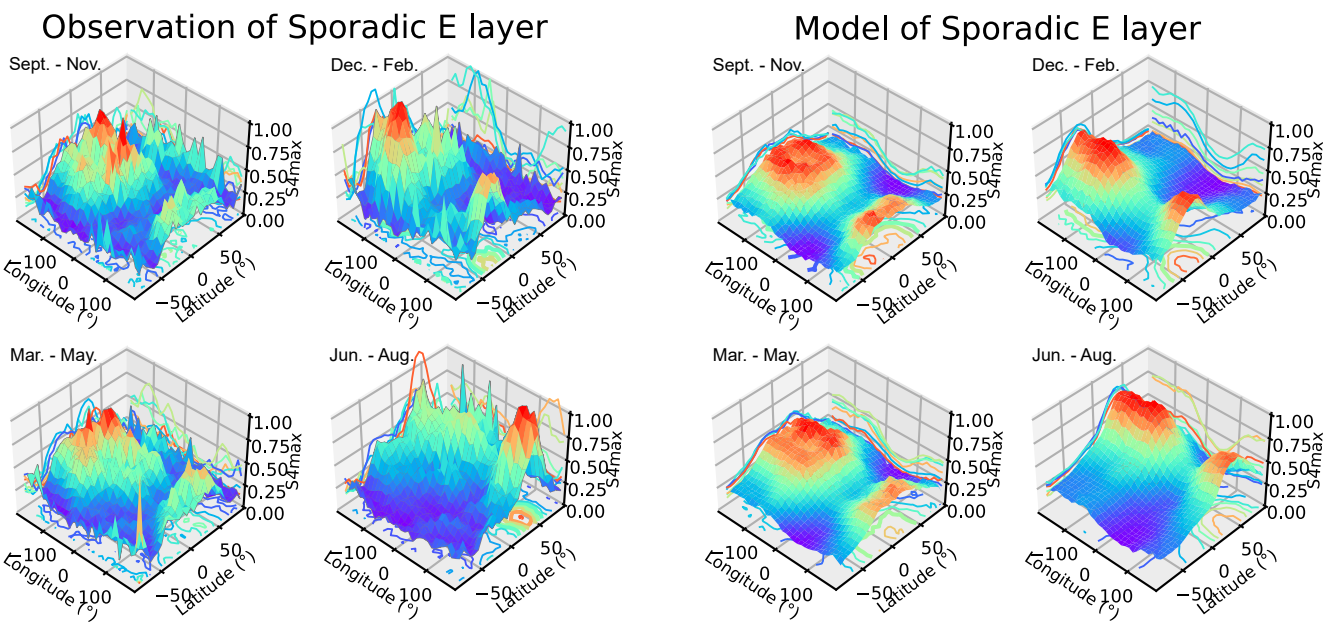

Figure 10. Global distributions of the intensity of E_s layers at 0 UT in the four seasons, represented by S4max from satellite radio occultation observations and the model outputs in the period 2006–2014. Plots for the autumn (September, October, and November) in the top left, the winter (December, January, and February) in the top right, the spring (March, April, and May) in the bottom left, and the summer (June, July, and August) in the bottom right.

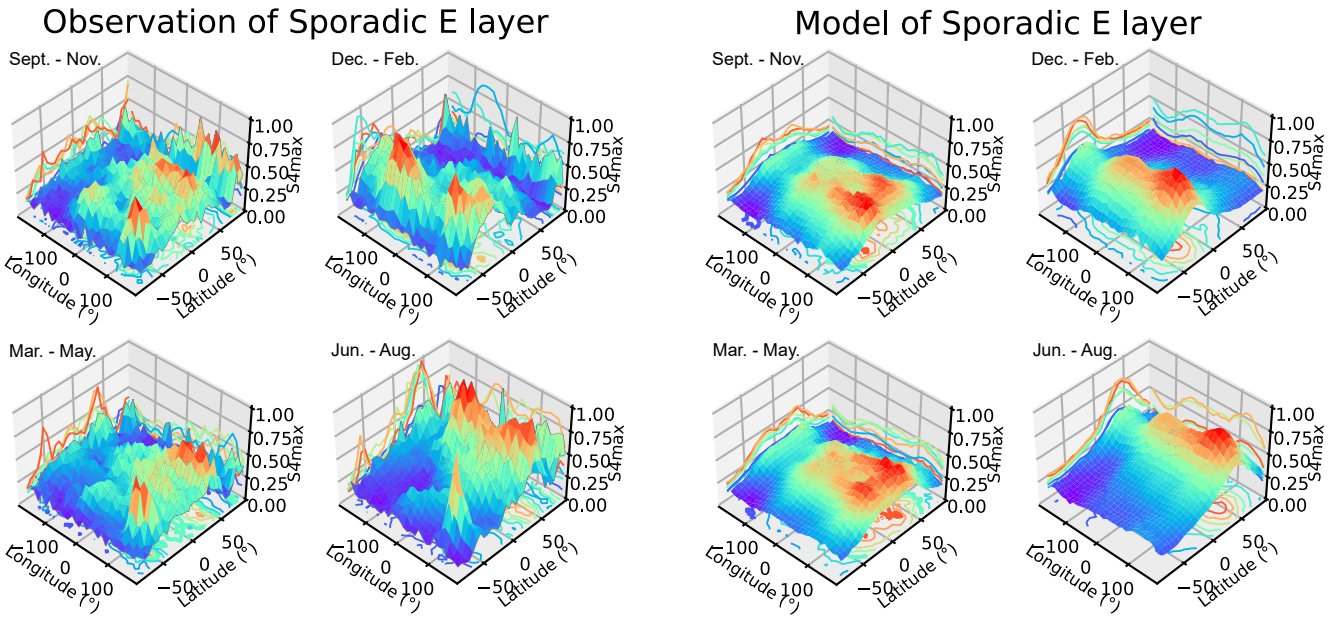

Figure 11. The same as Figure 10 but at 12 UT.

To further examine the model performance, the S4max from the model based on COSMIC satellite RO data was compared to the hourly manually scaled critical frequencies of E_s layers, f_oEs, obtained from a ground-based ionosonde at Beijing (40.3°N, 116.2°E). Figure 12 shows the density scatter plot of the hourly f_oEs from the Beijing ionosonde versus the hourly S4max model outputs in the period 2006–2014. The orange and white contour lines represent the number of data accounting for 50% and 90% satellite RO measurements. The red line represents a linear least-squares fit with the standard deviation from the mean within a 0.15 S4max band as an error, which yields the relation between f_oEs and S4max model outputs $f_oEs = 2.51 + 3.22\times$ S4max (correlation coefficient: $r = 0.52$, $p \ll 0.01$).

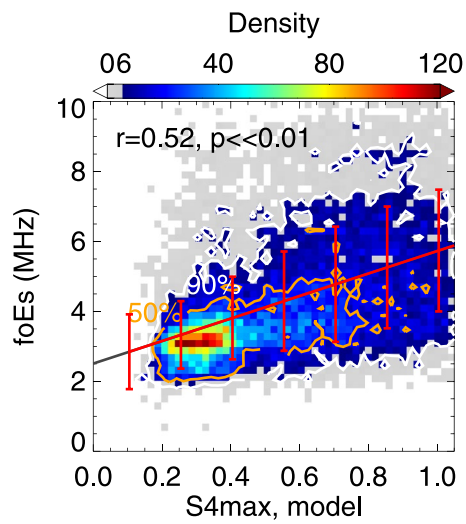

Figure 12. Density scatter plot of the hourly manually scaled f_oEs measured by an ionosonde at Beijing versus the hourly S4max model outputs in the period 2006–2014. The orange and white contour lines represent 50% and 90% of the number of data. The red line represents the linear least-squares fit with the standard deviation from the mean within a 0.15 S4max band.

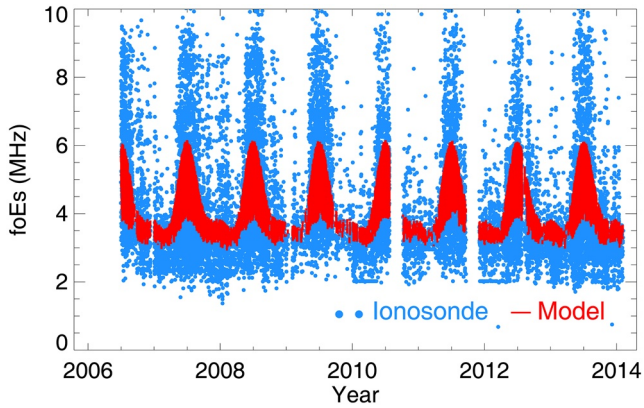

Figure 13. Comparison of the hourly f_oEs from the ionosonde observations at Beijing with the hourly f_oEs derived from the S4max model outputs by the fitting equation.

Figure 13 shows a comparison of the hourly f_oEs from the ionosonde observations at Beijing (blue) with the hourly f_oEs from the S4max model by the fitting equation $f_oEs = 2.51 + 3.22\times$ S4max (red). The E_s layer is more likely to be beyond the climatology in summer, possibly due to stronger vertical convergences of ions caused by wind shear, horizontal movement of metallic ions (Yu, Xue, et al., 2021), and significant dynamical/electromagnetic coupling between the lower and upper atmosphere (Davis & Johnson, 2005; Yu et al., 2015). The model can describe the diurnal and seasonal variations in E_s layers, but it cannot capture the significant variability of E_s layers during summer. The vertical shear effects on the midlatitude E_s layer formation are not included due to the lack of global high-resolution thermospheric wind measurements in the model.

Figure 14 shows the density scatter plot of the daily maximum f_oEs from the ionosonde at Beijing versus the daily maximum S4max model outputs in the period 2006–2014. The orange and white contour lines represent the number of data accounting for 50%, and 80% of satellite RO measurements. A linear relationship ($r = 0.68$, $p \ll 0.01$) between the f_oEs and S4max model outputs was found to be $f_oEs = 2.06 + 5.77\times$ S4max. The least-square fit is represented as a red line, with its uncertainty represented by the standard deviation. The results show that the model can describe the climatology of daily E_s layers, although the correlation between ionosonde observations and model outputs based on S4 from the COSMIC satellite RO data may be influenced by differences in the observational geometry of ground-based ionosondes and satellite RO measurements (Yue et al., 2016; Zeng & Sokolovskiy, 2010), as well as the local ionospheric variability within 1 day.

Figure 15 shows a comparison of the daily maximum f_oEs from the ionosonde observations at Beijing with the daily maximum f_oEs from the S4max model by the fitting equation. The model outputs of f_oEs are moderately correlated with f_oEs from the ionosonde. The difference between the observations and model primarily results from the "sporadic" characteristics of E_s layers represented by the deviations from the ionospheric climatology.

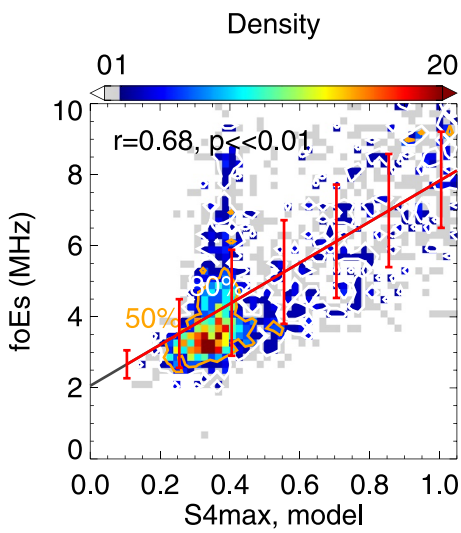

Figure 14. Density scatter plot of the daily maximum f_oEs measured by an ionosonde at Beijing versus the daily maximum S4max model outputs in the period 2006–2014. The orange and white contour lines represent 50% and 80% of the number of data. The red line represents the linear least-squares fit with the standard deviation from the mean within a 0.15 S4max band.

6. Discussion

Carmona et al. (2022) compared the observations of E_s layers from five different GPS-RO techniques (i.e., L1, L2 amplitude SNRs, and phase perturbations (Chu et al., 2014), L1 SNR (Arras & Wickert, 2018), TEC (Niu et al., 2019), excess phase and TEC (Gooch et al., 2020), and the maximum amplitude scintillation S4 index (S4max) (Yu et al., 2020)) against observations from ground-based ionosondes in the Global Ionosphere Radio Observatory network. Among the five techniques, the methodology by Yu et al. (2020) using the S4max index is one recommended method for studying the climatology of E_s layers, since it shows better agreement with measurements from ionosondes in most circumstances (Carmona et al., 2022). The intensity of E_s layers can be obtained from the S4max model outputs. Note that the linear regression equation between the f_oEs and S4max model outputs may be slightly different due to the geographic location and different types of ionosondes. The performance of the model may potentially be improved by combining the amplitude and phase of the L1/L2 signals in the GNSS RO data.

The S4max data from the GNSS RO measurements were used to describe the global variability of the E_s layer. The results presented here show that it is a practical approach to construct an empirical model of the climatology of E_s layers based on sufficiently large GNSS RO data. In Figures 10 and 11, we found that the E_s layers at high latitudes cause the most disagreements

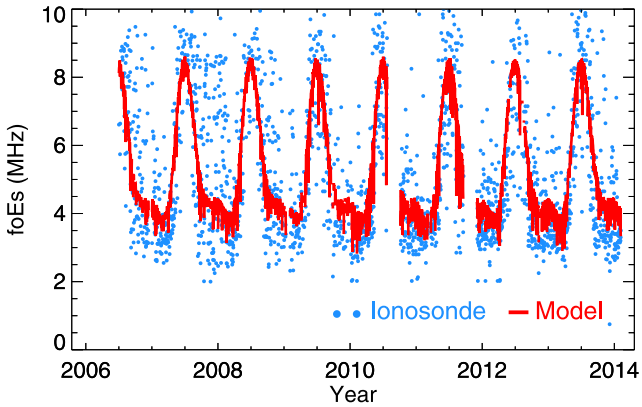

Figure 15. Comparison of the daily maximum f_oEs from the ionosonde observations at Beijing with the daily maximum f_oEs derived from the S4max model outputs by the fitting equation.

between the model outputs and the observations, although the morphology of E_s layers can be reproduced by the model. One shortcoming of the model is that it mainly describes the meridional movement of E_s layers in the latitudes of ±60° while the high-latitude E_s layers were not well defined in the latitudinal distribution of the model. Besides, the influences of solar activity, equatorial electrojet current plasma instabilities, and geomagnetic disturbances are not yet included in the model. The short-term variations in the low- and high-latitude E_s layers are associated with fast solar wind streams (Davies, 1990; L. Resende et al., 2021) and recurrent geomagnetic activity (Yu, Scott, Xue, Yue, Chi, et al., 2021).

The global morphology of E_s layers generally agrees with the morphology of VIC from the Horizontal Wind Model (Qiu et al., 2019). However, the comparison of hourly f_oEs values from ionosonde observations and average VIC using the GAIA model indicates that the large uncertainty in thermospheric winds from current numerical models makes accurate prediction of the E_s layer a technical challenge, due to the lack of high spatial-resolution global wind measurements in the mesosphere and lower thermosphere (Shinagawa et al., 2021). A recent study shows a good relationship between the E_s layer and the vertical wind shear measured from the Ionospheric Connection Explorer (Yamazaki et al., 2022). Therefore, we will address the shortcomings of the model in the future work by including more input factors (e.g., strong wind shears, solar activity, geomagnetic disturbances, lower atmosphere perturbations, and variations in meteor flux).

7. Conclusions

In this study, we have constructed an empirical model of the ionospheric E_s layer using the multivariable nonlinear least-squares-fitting method, based on S4max data retrieved from COSMIC satellite RO measurements in the period 2006–2014. The empirical model describes the intensity of E_s layers as a function of altitude, latitude, longitude, UT, and DOY. The model not only provides a global climatology of the intensity of E_s layers, but also captures the seasonal variations of E_s layers (Yu, Xue, et al., 2021) and the significant latitude dependence of the E_s layer, which occurs predominantly at midlatitudes (Tsai et al., 2018; Yu et al., 2019).

The S4max model outputs were compared to the hourly manually scaled observations of f_oEs from a ground-based ionosonde at Beijing. The model can reproduce the diurnal and seasonal variations in E_s layers, while the variability of E_s layers with a significant deviation from climatology during summer was not presented in the model. The correlation coefficient between the hourly f_oEs and the S4max model outputs in the period 2006–2014 is 0.52. The correlation coefficient between the daily maximum f_oEs and the S4max model outputs is 0.68. The largest discrepancies between the model and observations are at the high-latitude E_s layers. The differences result from the simplified spatial distribution of the E_s layer, especially for the latitudinal variation. In this study, we mainly focus on constructing a climatological model of the E_s layer. In future work, we will improve the model by incorporating more year-to-year variables, including Kp, F10.7 parameters, and wind fields.

Data Availability Statement

The Constellation Observing System for Meteorology, Ionosphere, and Climate (COSMIC) satellite radio occultation data are available from the COSMIC Data Analysis and Archive Center website (https://data.cosmic.ucar.edu/gnss-ro/). The ionosonde data are available from the Data Centre for Meridian Space Weather Monitoring Project (https://data.meridianproject.ac.cn/data-directory/) and the Geophysics Center, National Earth System Science Data Center at BNOSE, IGGCAS (http://wdc.geophys.ac.cn/dbView.asp?IonoPublish).

Acknowledgments
We acknowledge the Chinese Meridian Project, the Solar-Terrestrial Environment Research Network, the Geophysics Center, National Earth System Science Data Center at BNOSE, IGGCAS, and the National Space Science Data Center, National Science and Technology Infrastructure of China for providing the ionosonde data. The authors acknowledge the Constellation Observing System for Meteorology, Ionosphere, and Climate (COSMIC) Data Analysis and Archive Center for providing the COSMIC radio occultation data. The authors would like to thank the National Science and Technology Infrastructure of China. This work has been supported by the Project of Stable Support for Youth Team in Basic Research Field, CAS (grant No. YSBR-018), the National Natural Science Foundation of China (grant Nos. 42125402, 41974174, 42188101, and 41831071), the B-type Strategic Priority Program of CAS (grant no. XDB41000000), the Open Research Project of Large Research Infrastructures of CAS - "Study on the interaction between low/mid-latitude atmosphere and ionosphere based on the Chinese Meridian Project," the Joint Open Fund of Mengcheng National Geophysical Observatory (grant no. MENGO-202207), and the Fundamental Research Fund for the Central Universities. B. Yu was supported by the Royal Society for the Newton International Fellowship (grant no. NIF\R1\180815).

References

Anthes, R. A., Bernhardt, P., Chen, Y., Cucurull, L., Dymond, K., Ector, D., et al. (2008). The COSMIC/FORMOSAT-3 mission: Early results. *Bulletin of the American Meteorological Society*, *89*(3), 313–334. https://doi.org/10.1175/bams-89-3-313

Arras, C., Jacobi, C., & Wickert, J. (2009). Semidiurnal tidal signature in sporadic e occurrence rates derived from GPS radio occultation measurements at higher midlatitudes. In *Annales Geophysicae*, (Vol. 27(6), pp. 2555–2563). Copernicus GmbH. https://doi.org/10.5194/angeo-27-2555-2009

Arras, C., & Wickert, J. (2018). Estimation of ionospheric sporadic E intensities from GPS radio occultation measurements. *Journal of Atmospheric and Solar-Terrestrial Physics*, *171*, 60–63. https://doi.org/10.1016/j.jastp.2017.08.006

Arras, C., Wickert, J., Beyerle, G., Heise, S., Schmidt, T., & Jacobi, C. (2008). A global climatology of ionospheric irregularities derived from GPS radio occultation. *Geophysical Research Letters*, *35*(14), L14809. https://doi.org/10.1029/2008gl034158

Briggs, B., & Parkin, I. (1963). On the variation of radio star and satellite scintillations with zenith angle. *Journal of Atmospheric and Terrestrial Physics*, *25*(6), 339–366. https://doi.org/10.1016/0021-9169(63)90150-8

Cai, X., Yuan, T., & Eccles, J. V. (2017). A numerical investigation on tidal and gravity wave contributions to the summer time Na variations in the midlatitude E region. *Journal of Geophysical Research: Space Physics*, *122*(10), 10–577. https://doi.org/10.1002/2016ja023764

Cai, X., Yuan, T., Eccles, J. V., Pedatella, N., Xi, X., Ban, C., & Liu, A. Z. (2019). A numerical investigation on the variation of sodium ion and observed thermospheric sodium layer at Cerro Pachón, Chile during equinox. *Journal of Geophysical Research: Space Physics*, *124*(12), 10395–10414. https://doi.org/10.1029/2018ja025927

Carmona, R. A., Nava, O. A., Dao, E. V., & Emmons, D. J. (2022). A comparison of sporadic-E occurrence rates using GPS radio occultation and ionosonde measurements. *Remote Sensing*, *14*(3), 581. https://doi.org/10.3390/rs14030581

Chu, Y.-H., Wang, C., Wu, K., Chen, K., Tzeng, K., Su, C.-L., et al. (2014). Morphology of sporadic E layer retrieved from COSMIC GPS radio occultation measurements: Wind shear theory examination. *Journal of Geophysical Research: Space Physics*, *119*(3), 2117–2136. https://doi.org/10.1002/2013ja019437

Davies, K. (1990). *Ionospheric radio (No. 31)*. IET.

Davis, C. J., & Johnson, C. G. (2005). Lightning-induced intensification of the ionospheric sporadic E layer. *Nature*, *435*(7043), 799–801. https://doi.org/10.1038/nature03638

Fernandez-Prades, C., Presti, L. L., & Falletti, E. (2011). Satellite radiolocalization from GPS to GNSS and beyond: Novel technologies and applications for civil mass market. *Proceedings of the IEEE*, *99*(11), 1882–1904. https://doi.org/10.1109/jproc.2011.2158032

Gooch, J. Y., Colman, J. J., Nava, O. A., & Emmons, D. J. (2020). Global ionosonde and GPS radio occultation sporadic-E intensity and height comparison. *Journal of Atmospheric and Solar-Terrestrial Physics*, *199*, 105200. https://doi.org/10.1016/j.jastp.2020.105200

Guo, Y., & Liu, A. Z. (2021). Seasonal variation of vertical heat and energy fluxes due to dissipating gravity waves in the mesopause region over the Andes. *Journal of Geophysical Research: Atmospheres*, *126*(3), e2020JD033825. https://doi.org/10.1029/2020jd033825

Haldoupis, C. (2011). A tutorial review on sporadic E layers. *Aeronomy of the Earth's Atmosphere and Ionosphere*, 381–394. https://doi.org/10.1007/978-94-007-0326-1_29

Hu, L., Ning, B., Liu, L., Zhao, B., Chen, Y., & Li, G. (2014). Comparison between ionospheric peak parameters retrieved from COSMIC measurement and ionosonde observation over Sanya. *Advances in Space Research*, *54*(6), 929–938. https://doi.org/10.1016/j.asr.2014.05.012

Jakowski, N., Hoque, M., & Mayer, C. (2011). A new global TEC model for estimating transionospheric radio wave propagation errors. *Journal of Geodesy*, *85*(12), 965–974. https://doi.org/10.1007/s00190-011-0455-1

Kakinami, Y., Watanabe, S., & Oyama, K.-I. (2008). An empirical model of electron density in low latitude at 600 Km obtained by Hinotori satellite. *Advances in Space Research*, *41*(9), 1495–1499. https://doi.org/10.1016/j.asr.2007.09.031

Kopp, E. (1997). On the abundance of metal ions in the lower ionosphere. *Journal of Geophysical Research*, *102*(A5), 9667–9674. https://doi.org/10.1029/97ja00384

Koto, S., Aso, T., Horiuchi, T., Nakamura, J., & Matsuoka, T. (1972). Sporadic-E formation by wind shear, comparison between observation and theory. *Radio Science*, *7*(3), 359–362. https://doi.org/10.1029/rs007i003p00359

Liu, A. Z., Lu, X., & Franke, S. J. (2013). Diurnal variation of gravity wave momentum flux and its forcing on the diurnal tide. *Journal of Geophysical Research: Atmospheres*, *118*(4), 1668–1678. https://doi.org/10.1029/2012jd018653

Liu, Y., Zhou, C., Tang, Q., Li, Z., Song, Y., Qing, H., et al. (2018). The seasonal distribution of sporadic E layers observed from radio occultation measurements and its relation with wind shear measured by TIMED/TIDI. *Advances in Space Research*, *62*(2), 426–439. https://doi.org/10.1016/j.asr.2018.04.026

Liu, Z., Fang, H., Hoque, M. M., Weng, L., Yang, S., & Gao, Z. (2019). A new empirical model of NmF2 based on CHAMP, GRACE, and COSMIC radio occultation. *Remote Sensing*, *11*(11), 1386. https://doi.org/10.3390/rs11111386

Liu, Z., Fang, H., Yue, X., & Lyu, H. (2021). Wavenumber-4 patterns of the sporadic E over the middle-and low-latitudes. *Journal of Geophysical Research: Space Physics*, *126*(8), e2021JA029238. https://doi.org/10.1029/2021ja029238

Liu, Z., Li, Q., Fang, H., & Gao, Z. (2021). Longitudinal structure in the altitude of the sporadic E observed by COSMIC in low-latitudes. *Remote Sensing*, *13*(22), 4714. https://doi.org/10.3390/rs13224714

Mathews, J. (1998). Sporadic E: Current views and recent progress. *Journal of Atmospheric and Solar-Terrestrial Physics*, *60*(4), 413–435. https://doi.org/10.1016/s1364-6826(97)00043-6

Mathews, J. D., Sulzer, M. P., & Perillat, P. (1997). Aspects of layer electrodynamics inferred from high-resolution ISR observations of the 80–270 Km ionosphere. *Geophysical Research Letters*, *24*(11), 1411–1414. https://doi.org/10.1029/97gl01320

Niu, J. (2021a). Difference in the sporadic E layer occurrence ratio between the southern and northern low magnetic latitude regions as observed by COSMIC radio occultation data. *Space Weather*, *19*(4), e2020SW002635. https://doi.org/10.1029/2020sw002635

Niu, J. (2021b). Relationship between wavenumber 4 pattern of sporadic E layer intensity and eastward propagating diurnal tide with zonal wavenumber 3 in low latitude region. *Journal of Geophysical Research: Space Physics*, *126*(6), e2020JA028985. https://doi.org/10.1029/2020ja028985

Niu, J., Weng, L., Meng, X., & Fang, H. (2019). Morphology of ionospheric sporadic E layer intensity based on cosmic occultation data in the midlatitude and low-latitude regions. *Journal of Geophysical Research: Space Physics*, *124*(6), 4796–4808. https://doi.org/10.1029/2019ja026828

Pancheva, D., Haldoupis, C., Meek, C., Manson, A., & Mitchell, N. (2003). Evidence of a role for modulated atmospheric tides in the dependence of sporadic E layers on planetary waves. *Journal of Geophysical Research*, *108*(A5), 1176. https://doi.org/10.1029/2002ja009788

Pignalberi, A., Pezzopane, M., & Zuccheretti, E. (2014). Sporadic E layer at mid-latitudes: Average properties and influence of atmospheric tides. In *Annales Geophysicae* (Vol. 32(11), pp. 1427–1440). Copernicus GmbH. https://doi.org/10.5194/angeo-32-1427-2014

Pignalberi, A., Pezzopane, M., & Zuccheretti, E. (2015). A spectral study of the mid-latitude sporadic E layer characteristic oscillations comparable to those of the tidal and the planetary waves. *Journal of Atmospheric and Solar-Terrestrial Physics*, *122*, 34–44. https://doi.org/10.1016/j.jastp.2014.10.017

Plane, J. M. (2012). Cosmic dust in the Earth's atmosphere. *Chemical Society Reviews*, *41*(19), 6507–6518. https://doi.org/10.1039/c2cs35132c
Plane, J. M., Feng, W., & Dawkins, E. C. (2015). The mesosphere and metals: Chemistry and changes. *Chemical Reviews*, *115*(10), 4497–4541. https://doi.org/10.1021/cr500501m
Qiu, L., Yu, T., Yan, X., Sun, Y.-Y., Zuo, X., Yang, N., et al. (2021). Altitudinal and latitudinal variations in ionospheric sporadic-E layer obtained from FORMOSAT-3/COSMIC radio occultation. *Journal of Geophysical Research: Space Physics*, *126*(9), e2021JA029454. https://doi.org/10.1029/2021ja029454
Qiu, L., Zuo, X., Yu, T., Sun, Y., Liu, H., Sun, L., & Zhao, B. (2021). The characteristics of summer descending sporadic E layer observed with the ionosondes in the China region. *Journal of Geophysical Research: Space Physics*, *126*(3), e2020JA028729. https://doi.org/10.1029/2020ja028729
Qiu, L., Zuo, X., Yu, T., Sun, Y., & Qi, Y. (2019). Comparison of global morphologies of vertical ion convergence and sporadic E occurrence rate. *Advances in Space Research*, *63*(11), 3606–3611. https://doi.org/10.1016/j.asr.2019.02.024
Resende, L., Zhu, Y., Denardini, C., Batista, I., Shi, J., Moro, J., et al. (2021). New findings of the sporadic E (Es) layer development around the magnetic equator during a High-Speed Solar (HSS) wind stream event. *Journal of Geophysical Research: Space Physics*, *126*(9), e2021JA029416. https://doi.org/10.1029/2021ja029416
Resende, L. C. A., Arras, C., Batista, I. S., Denardini, C. M., Bertollotto, T. O., & Moro, J. (2018). Study of sporadic E layers based on GPS radio occultation measurements and digisonde data over the Brazilian region. In *Annales Geophysicae* (Vol. 36(2), pp. 587–593). Copernicus GmbH. https://doi.org/10.5194/angeo-36-587-2018
Šauli, P., & Bourdillon, A. (2008). Height and critical frequency variations of the sporadic-E layer at midlatitudes. *Journal of Atmospheric and Solar-Terrestrial Physics*, *70*(15), 1904–1910. https://doi.org/10.1016/j.jastp.2008.03.016
Schreiner, W., Rocken, C., Sokolovskiy, S., Syndergaard, S., & Hunt, D. (2007). Estimates of the precision of GPS radio occultations from the COSMIC/FORMOSAT-3 mission. *Geophysical Research Letters*, *34*(4), L04808. https://doi.org/10.1029/2006gl027557
Schreiner, W., Sokolovskiy, S., Hunt, D., Rocken, C., & Kuo, Y.-H. (2011). Analysis of GPS radio occultation data from the FORMOSAT-3/COSMIC and Metop/GRAS missions at CDAAC. *Atmospheric Measurement Techniques*, *4*(10), 2255–2272. https://doi.org/10.5194/amt-4-2255-2011
Shinagawa, H., Miyoshi, Y., Jin, H., & Fujiwara, H. (2017). Global distribution of neutral wind shear associated with sporadic E layers derived from GAIA. *Journal of Geophysical Research: Space Physics*, *122*(4), 4450–4465. https://doi.org/10.1002/2016ja023778
Shinagawa, H., Tao, C., Jin, H., Miyoshi, Y., & Fujiwara, H. (2021). Numerical prediction of sporadic E layer occurrence using GAIA. *Earth Planets and Space*, *73*(1), 1–18. https://doi.org/10.1186/s40623-020-01330-y
Tang, Q., Zhao, J., Yu, Z., Liu, Y., Hu, L., Zhou, C., et al. (2021). Occurrence and variations of middle and low latitude sporadic E layer investigated with longitudinal and latitudinal chains of ionosondes. *Space Weather*, *19*(12), e2021SW002942. https://doi.org/10.1029/2021SW002942
Tang, Q., Zhou, C., Liu, H., Liu, Y., Zhao, J., Yu, Z., et al. (2021). The possible role of turbopause on sporadic-E layer formation at middle and low latitudes. *Space Weather*, *19*(12), e2021SW002883. https://doi.org/10.1029/2021sw002883
Tsai, L.-C., Su, S.-Y., Liu, C.-H., Schuh, H., Wickert, J., & Alizadeh, M. M. (2018). Global morphology of ionospheric sporadic E layer from the FormoSat-3/COSMIC GPS radio occultation experiment. *GPS Solutions*, *22*(4), 1–12. https://doi.org/10.1007/s10291-018-0782-2
Weber, E., Tsunoda, R., Buchau, J., Sheehan, R., Strickland, D., Whiting, W., & Moore, J. (1985). Coordinated measurements of auroral zone plasma enhancements. *Journal of Geophysical Research*, *90*(A7), 6497–6513. https://doi.org/10.1029/ja090ia07p06497
Whitehead, J. (1961). The Formation of the sporadic-E layer in the temperate zones. *Journal of Atmospheric and Terrestrial Physics*, *20*(1), 49–58. https://doi.org/10.1016/0021-9169(61)90097-6
Whitehead, J. (1970). Production and prediction of sporadic E. *Reviews of Geophysics*, *8*(1), 65–144. https://doi.org/10.1029/rg008i001p00065
Whitehead, J. (1989). Recent work on mid-latitude and equatorial sporadic-E. *Journal of Atmospheric and Terrestrial Physics*, *51*(5), 401–424. https://doi.org/10.1016/0021-9169(89)90122-0
Wu, D. L., Ao, C. O., Hajj, G. A., de La Torre Juarez, M., & Mannucci, A. J. (2005). Sporadic E morphology from GPS-CHAMP radio occultation. *Journal of Geophysical Research*, *110*(A1), A01306. https://doi.org/10.1029/2004ja010701
Wu, J., Feng, W., Liu, H.-L., Xue, X., Marsh, D. R., & Plane, J. M. C. (2021). Self-consistent global transport of metallic ions with WACCM-X. *Atmospheric Chemistry and Physics*, *21*(20), 15619–15630. https://doi.org/10.5194/acp-21-15619-2021
Yamazaki, Y., Arras, C., Andoh, S., Miyoshi, Y., Shinagawa, H., Harding, B., et al. (2022). Examining the wind shear theory of sporadic E with ICON/MIGHTI winds and COSMIC-2 radio occultation data. *Geophysical Research Letters*, *49*(1), e2021GL096202. https://doi.org/10.1029/2021gl096202
Yu, B., Scott, C. J., Xue, X., Yue, X., Chi, Y., Dou, X., & Lockwood, M. (2021). A signature of 27 Day solar rotation in the concentration of metallic ions within the terrestrial ionosphere. *The Astrophysical Journal*, *916*(2), 106. https://doi.org/10.3847/1538-4357/ac0886
Yu, B., Scott, C. J., Xue, X., Yue, X., & Dou, X. (2020). Derivation of global ionospheric sporadic E critical frequency (f_o Es) data from the amplitude variations in GPS/GNSS radio occultations. *Royal Society Open Science*, *7*(7), 200320. https://doi.org/10.1098/rsos.200320
Yu, B., Scott, C. J., Xue, X., Yue, X., & Dou, X. (2021). Using GNSS radio occultation data to derive critical frequencies of the ionospheric sporadic E layer in real time. *GPS Solutions*, *25*(1), 1–11. https://doi.org/10.1007/s10291-020-01050-6
Yu, B., Xue, X., Lu, G., Ma, M., Dou, X., Qie, X., et al. (2015). Evidence for lightning-associated enhancement of the ionospheric sporadic E layer dependent on lightning stroke energy. *Journal of Geophysical Research: Space Physics*, *120*(10), 9202–9212. https://doi.org/10.1002/2015ja021575
Yu, B., Xue, X., Scott, C. J., Wu, J., Yue, X., Feng, W., et al. (2021). Interhemispheric transport of metallic ions within ionospheric sporadic E layers by the lower thermospheric meridional circulation. *Atmospheric Chemistry and Physics*, *21*(5), 4219–4230. https://doi.org/10.5194/acp-21-4219-2021
Yu, B., Xue, X., Yue, X., Yang, C., Yu, C., Dou, X., et al. (2019). The global climatology of the intensity of the ionospheric sporadic E layer. *Atmospheric Chemistry and Physics*, *19*(6), 4139–4151. https://doi.org/10.5194/acp-19-4139-2019
Yuan, T., Wang, J., Cai, X., Sojka, J., Rice, D., Oberheide, J., & Criddle, N. (2014). Investigation of the seasonal and local time variations of the high-altitude sporadic Na layer (Nas) formation and the associated midlatitude descending E layer (Es) in lower E region. *Journal of Geophysical Research: Space Physics*, *119*(7), 5985–5999. https://doi.org/10.1002/2014ja019942
Yue, X., Schreiner, W., Zeng, Z., Kuo, Y.-H., & Xue, X. (2015). Case study on complex sporadic E layers observed by GPS radio occultations. *Atmospheric Measurement Techniques*, *8*(1), 225–236. https://doi.org/10.5194/amt-8-225-2015
Yue, X., Schreiner, W. S., Pedatella, N., Anthes, R. A., Mannucci, A. J., Straus, P. R., & Liu, J.-Y. (2014). Space weather observations by GNSS radio occultation: From FORMOSAT-3/COSMIC to FORMOSAT-7/COSMIC-2. *Space Weather*, *12*(11), 616–621. https://doi.org/10.1002/2014sw001133
Yue, X., Schreiner, W. S., Pedatella, N. M., & Kuo, Y.-H. (2016). Characterizing GPS radio occultation loss of lock due to ionospheric weather. *Space Weather*, *14*(4), 285–299. https://doi.org/10.1002/2015sw001340
Zeng, Z., & Sokolovskiy, S. (2010). Effect of sporadic E clouds on GPS radio occultation signals. *Geophysical Research Letters*, *37*(18), L18817. https://doi.org/10.1029/2010gl044561